PERFORMANCE OF 4-STATE MDPSK TRELLIS CODES IN SHADOWED FADING MOBILE COMMUNICATION CHANNELS

Eman Fahmi, Shawki Shaaban and Hassan Kheirallah

Department of Electrical Engineering, Faculty of Engineering,
Alexandria University, Alexandria, Egypt.

ABSTRACT

The performance of convolutionally 4-state **MDPSK** **T**rellis-**C**oded **M**odulation **(TCM)** codes using a combination of one-bit and two-bit **differential detectors** and a **Viterbi** decoder for digital speech transmission over fading channels is determined. In this paper, we present four 4-state **MDPSK TCM** schemes, the first is a 4-state **4-DPSK** trellis code, the second and the third are 4-state **8-DPSK** trellis codes with and without parallel paths respectively and the fourth is a 4-state **8-DPSK** trellis code without parallel paths and whose code has maximum product of the squared branch distances along the shortest error event path. Digital computer simulation is used to compare the performance of the considered **TCM** schemes in **Rayleigh** fading and in different degree of **shadowed Rician** fading channels. The simulation results show the **superiority** of the 4-state **8-DPSK** trellis code with maximum product of the squared branch distances and without parallel paths for bit error probabilities of 10^{-3} or less.

1. INTRODUCTION

Trellis-Coded Modulation **(TCM)** can be viewed as a combined coding and modulation technique for digital transmission over band-limited channels [1]. The modulation is embedded into the encoding process and is designed in conjunction with a rate n/n+1 convolutional code. Signal waveforms representing information sequences are designed to have large distance in **Euclidean** signal space.

TCM schemes are originally developed for additive white Gaussian noise **AWGN** channels [2]. **TCM** techniques allow the achievement of significant coding gains over conventional uncoded multilevel modulation without compromising bandwidth efficiency [3-4].

The common use of **TCM** techniques is in order to permit satisfactory operation at lower signal-to-noise ratios.

The performance of 4-state **QPSK** scheme in **Rician** fading channel was investigated in [5], while that of the **π/4-DQPSK** in **Rayleigh** fading and Gaussian noise was illustrated in [6]. The convolutionally interleaved **PSK** and **DPSK** trellis codes have been proposed in [7], for shadowed, fast fading mobile satellite channels.

The mobile radio channel is characterized by multiple signal paths between the transmitter and receiver due to reflections from buildings, terrain, and other scattering structures. This causes signal fading [8]. The rate at which the signal envelope fades is directly proportional to the speed of the mobile receiver. Analytically, this observation manifests itself as a **Doppler** frequency shift associated with each component. In this case, the channel is modeled as **Rayleigh** [9]. Alternatively, the channel is modeled as **Rician**, when a line-of-sight **(LOS)** component, $\mathbf{z_c}$ of unity power, $\mathbf{z_c^2 / 2 = 1}$, is added to the Rayleigh fading. **Shadowed Rician** fading model is obtained when the **(LOS)** component, $\mathbf{z_k}$ is subjected to a lognormal transformation. This transformation represents the effect of foliage attenuation or blockage, also referred to as shadowing [10].

In the following analysis, it is assumed that the receiver performs **differential** detection and the effect of the fading on the phase of the received signal is fully compensated.

A combination of one-bit and two-bit differential detectors is used at the receiving end to improve the performance of differentially detected **TCM**.

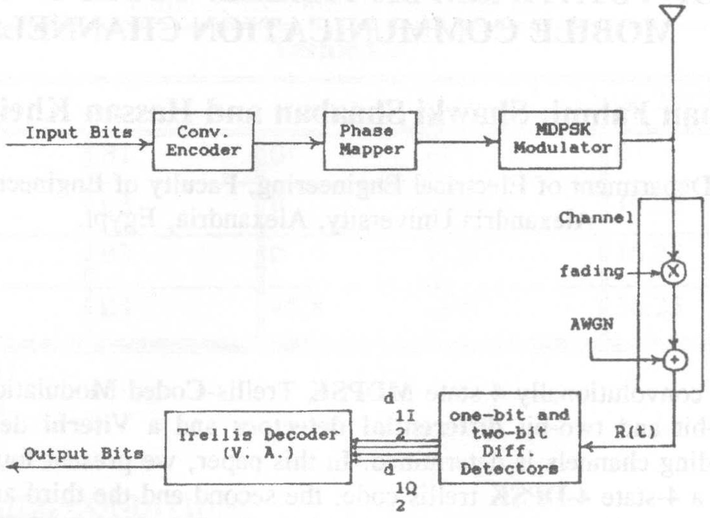

Figure 1. A block diagram of TCM schemes over fading channels.

2. SYSTEM MODEL AND CODE DESIGN:

Figure (1) represents a block diagram of a **TCM** scheme over mobile fading channels. The input bits are encoded by a convolutional encoder. The transmitter consists of a convolutional encoder, a phase mapper and a **MDPSK** modulator. In the communication channel, the transmitted signal is **faded** and corrupted by an **AWGN**. At the receiver the in-phase and quadrature components of the received signal are demodulated, quantized for soft decision. Using these quantized components, the **Viterbi** decoder detects the transmitted sequence based on maximum likelihood estimation.

The appropriate criterion for designing good **TCM** schemes is to **maximize** the minimum Euclidean distance between any two distinct information sequences of the coded signals.

The phase mapper converts the code binary sequence into M-ary PSK symbols as follows

$$C_k = e^{j\Delta\theta_k} \qquad (1)$$

The symbols C_k are differentially encoded and then modulated. The transmitted signal is given by

$$s_o(t) = \cos(\omega_c t + \theta_k) \qquad kT < t \le (k+1)T \quad (2)$$

where $\theta_k = \Delta\theta_k \oplus \theta_{k-1}$ mod 2 π.

The phase difference $\Delta\theta_k$ for 4-state **4DPSK** can expressed as

$$\Delta\theta_k = \theta_k - \theta_{k-1} = m(k)\ \pi/2,$$

where m(k) = 0, 1, 2, or 3.

The relevant distances between signals are $\Delta_1 = \sqrt{2}$, $\Delta_2 = 2$ and $\Delta_3 = \sqrt{2}$. The angle no. $0 \equiv 0°$, $1 \equiv 90°$, $2 \equiv 180°$, $3 \equiv 270°$. Figure (2 shows the state transition diagram for coded 4P modulation with four trellis states.

The 4-state 8PSK schemes employ redund nonbinary modulation in combination with a finite-st encoder which governs the selection of modulat signals to generate coded signal sequences [11].

The phase difference for 4-state 8DPSK can expressed as

$$\Delta\theta_k = \theta_k - \theta_{k-1} = B(k)\ \pi/8,$$

where B(k) = 1, 3, 5, 7, 9, 11, 13, or 15.

The relevant distances between signals are $\Delta_1 = 0.$ $\Delta_2 = \sqrt{2}$, $\Delta_3 = 1.848$ and $\Delta_4 = 2$. The angle no. $0 \equiv 15\pi/8$, $1 \equiv \pi/8$, $2 \equiv 3\pi/8$,... The state transition diagram is shown in Figure (2- it contains parallel paths, which imply that single sig

error events can occur. This limits the achievable shortest error event length to one. The trellis branches are labeled with redundant nonbinary modulation signals which have a good **Euclidean** distance.

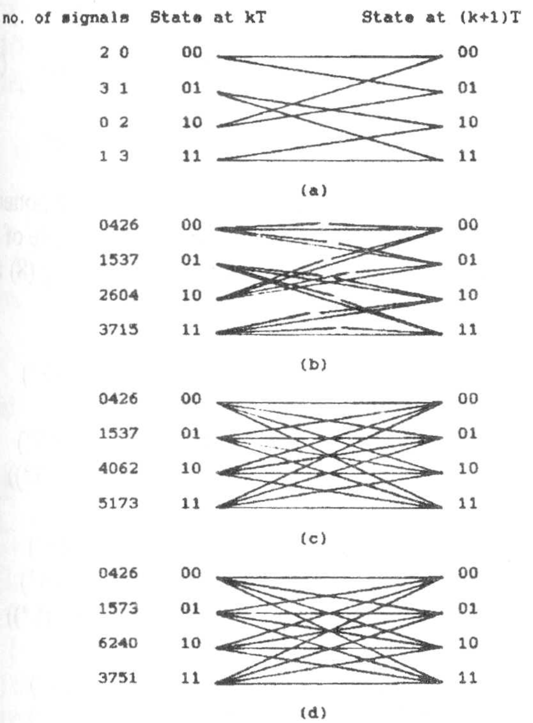

Fig. 2. State transition diagrams.

(a) Ungerboeck's 4-state 4PSK trellis diagram.

(b) Ungerboeck's 4-state 8PSK trellis diagram.

(c) The trellis diagram of a 4-state 8PSK trellis code without parallel paths.

(d) The trellis diagram of 4-state 8PSK trellis code without parallel paths for mobile fading channels.

Figure 2. State transition diagrams.

To increase the shortest error event length, parallel paths must be avoided. The trellis diagram of the 4-state **8PSK** trellis code **without** parallel paths is shown in Figure (2-c).

As it is seen, this diagram is fully connected and provides the shortest error event paths of length two.

To design good **TCM** codes over the fading channels, the shortest error event length, as well as the **product** of the squared branch distances along that path, should be **maximized**, as shown in Figure (2-d).

The code of Figure (2-c) has been designed to increase the shortest error event path length. However, its product of the squared branch distances along this path has not been optimized. In this work, we shall introduce another **4**-state trellis codes based on maximizing the product of the squared branch distances. Using set partitioning [1], the signal set of the **8PSK** can be partitioned into two subsets C_0 = (0, 2, 4, 6) and C_1 = (1, 3, 5, 7) with intraset distances Δ_2 and Δ_4. The "state difference" can be defined as the number of bits in which two states differ. Branches diverging from each state are associated with signals from subsets C_o or C_1 such that the distance between a pair of branches diverging from one state to two consecutive states with "state differences" two or one, is Δ_2 or Δ_4, respectively. The signals with distances Δ_3 are associated with branches remerging to a state from two consecutive states with "state difference" of two. The pair of paths remerging to a state from two states with "state difference" of one may be associated with signals with distances Δ_1 or Δ_3. The trellis diagram of the generated code is shown in Figure (2-d).

3. RECEIVER PERFORMANCE ANALYSIS AND SIMULATION RESULTS

The received signal is faded and corrupted by an **AWGN**. To represent the fading model in mathematical terms, that will be used in the computer simulation, computation of normally distributed (Gaussian) random variates is needed [12]. See Appendix **A**.

The received phasor may be expressed in **Rayleigh** fading as

$$R_k = [v_k + ju_k] \exp (j\theta_k) + N_k, \tag{5}$$

and in **shadowed Rician** fading as

$$R_k = [z_k + v_k + ju_k] \exp (j\theta_k) + N_k. \tag{6}$$

where

N_k is the additive white Gaussian noise **(AWGN)** with zero mean, and variance N_o,

θ_k is the transmitted phase angle,

v_k and u_k are the **Rayleigh** multipath components, they are independent and Gaussian [13], with zero mean and variance b_0, and

z_k is the lognormal, **LOS** component of the fading process, with mean μ_0 and variance d_0.

The received signal is differentially demodulated. The detection process is performed to estimate the transmitted signal from the **faded** received symbol. Bit errors are then counted to obtain an estimate of the bit error rate performance for a given value of $\mathbf{E_b / N_o}$.

The received signal at the sample $\mathbf{t = kT}$ can be expressed in **Rayleigh** fading as

$$R(kT) = v(kT)\cos(\omega_c kT+\theta_k) - u(kT)\sin(\omega_c kT+\theta_k) + n_o(kT), \qquad (7)$$

and in **shadowed Rician** fading as

$$R(kT) = z(kT)\cos(\omega_c kT + \theta_k) + v(kT)\cos(\omega_c kT+\theta_k) - u(kT)\sin(\omega_c kT+\theta_k) + n_o(kT), \qquad (8)$$

where

$$n_o(kT) = n_c(kT)\cos(\omega_c kT) - n_s(kT)\sin(\omega_c kT) \qquad (9)$$

Delaying the signal of eq. (7) by a **T** second and shifting the carrier by $\pm\pi/4$ yields

$$R(kT-T)_{\pm 45^\circ} = v(kT-T)\{\cos(\omega_c(kT-T)+\theta(kT-T)\pm 45^\circ)\} - u(kT-T)\{\sin(\omega_c(kT-T)+\theta(kT-T)\pm 45^\circ)\} + n_o(kT-T)_{\pm 45^\circ}. \qquad (10)$$

Similarly, for eq. (8)

$$R(kT-T)_{\pm 45^\circ} = z(kT-T)\{\cos(\omega_c(kT-T)+\theta(kT-T)\pm 45^\circ)\} + v(kT-T)\{\cos(\omega_c(kT-T)+\theta(kT-T)\pm 45^\circ)\} - u(kT-T)\{\sin(\omega_c(kT-T)+\theta(kT-T)\pm 45^\circ)\} + n_o(kT-T)_{\pm 45^\circ}, \qquad (11)$$

where

$$n_o(kT-T)_{\pm 45^\circ} = n_c(kT-T)\{\cos(\omega_c(kT-T) \pm 45^\circ)\} - n_s(kT-T)\{\sin(\omega_c(kT-T) \pm 45^\circ)\}. \qquad (12)$$

The outputs from the differential detectors are given by

$$d_{1I}(kT) = LP\{R(kT)\,R(kT-T)\}_{+45^\circ}$$

$$d_{1Q}(kT) = LP\{R(kT)\,R(kT-T)\}_{-45^\circ}$$

$$d_{2I}(kT) = LP\{R(kT)\,R(kT-2T)\}_{+45^\circ}$$

$$d_{2Q}(kT) = LP\{R(kT)\,R(kT-2T)\}_{-45^\circ}$$

where **LP** denotes taking the lowpass component. Taking the carrier frequency as integer multiple of the bit rate, and after some manipulation, using eq (8) and eq. (11), we get

$$\begin{aligned}\underset{Q}{d_{1I}}(kT) = {} & 1/2\, z_k z_{k-1}\cos(\theta_k - \theta_{k-1} \mp 45^\circ) \\ & + 1/2\, z_k v_{k-1}\cos(\theta_k - \theta_{k-1} \mp 45^\circ) \\ & - 1/2\, z_k u_{k-1}\sin(-(\theta_k-\theta_{k-1} \mp 45^\circ)) \\ & + 1/2\, v_k z_{k-1}\cos(\theta_k - \theta_{k-1} \mp 45^\circ) \\ & + 1/2\, v_k v_{k-1}\cos(\theta_k - \theta_{k-1} \mp 45^\circ) \\ & - 1/2\, v_k u_{k-1}\sin(-(\theta_k - \theta_{k-1} \mp 45^\circ)) \\ & - 1/2\, u_k z_{k-1}\sin(\theta_k - \theta_{k-1} \mp 45^\circ) \\ & - 1/2\, u_k v_{k-1}\sin(\theta_k - \theta_{k-1} \mp 45^\circ) \\ & + 1/2\, u_k u_{k-1}\cos(\theta_k - \theta_{k-1} \mp 45^\circ) \\ & + \sum_{L=1}^{4}\{n_L(kT)\, n'_L(kT-T)\}_{\pm 45^\circ}, \end{aligned} \qquad (14\text{-}(a,$$

$$\begin{aligned}\underset{Q}{d_{2I}}(kT) = {} & 1/2\, z_k z_{k-2}\cos(\theta_k - \theta_{k-2} \mp 45^\circ) \\ & + 1/2\, z_k v_{k-2}\cos(\theta_k - \theta_{k-2} \mp 45^\circ) \\ & - 1/2\, z_k u_{k-2}\sin(-(\theta_k - \theta_{k-2} \mp 45^\circ)) \\ & + 1/2\, v_k z_{k-2}\cos(\theta_k - \theta_{k-2} \mp 45^\circ) \\ & + 1/2\, v_k v_{k-2}\cos(\theta_k - \theta_{k-2} \mp 45^\circ) \\ & - 1/2\, v_k u_{k-2}\sin(-(\theta_k - \theta_{k-2} \mp 45^\circ)) \\ & - 1/2\, u_k z_{k-2}\sin(\theta_k - \theta_{k-2} \mp 45^\circ) \\ & - 1/2\, u_k v_{k-2}\sin(\theta_k - \theta_{k-2} \mp 45^\circ) \\ & + 1/2\, u_k u_{k-2}\cos(\theta_k - \theta_{k-2} \mp 45^\circ) \\ & + \sum_{L=1}^{4}\{n_L(kT)\, n'_L(kT-2T)\}_{\pm 45^\circ}, \end{aligned} \qquad (14\text{-}($$

where

$$\sum_{L=1}^{4} \{n_L(kT)\, n'_L(kT-2T)\}_{\pm 45°} = [1/2\, z_k \cos(\pm 45° - \theta_k)$$
$$+ 1/2\, v_k \cos(\pm\, 45° - \theta_k) + 1/2\, u_k \sin(\pm\, 45° - \theta_k)$$
$$+ 1/2\, n_{ck} \cos(\pm\, 45°) + 1/2\, n_{sk} \sin(\pm\, 45°)] \quad \mathbf{n_{c\,k-1}}$$
$$+ [-1/2\ z_k\ \sin(\pm\, 45° - \theta_k)$$
$$- 1/2\, v_k \sin(\pm\, 45° - \theta_k) + 1/2\, u_k \cos(\pm\, 45° - \theta_k)$$
$$- 1/2\, n_{ck} \sin(\pm\, 45°) + 1/2\, n_{sk} \cos(\pm\, 45°\ ] \quad \mathbf{n_{s\,k-1}}$$

$$+ 1/2\, \mathbf{n_{c\,k}}\ [z_{k-1} \cos(-\theta_{k-1} - (\pm\, 45°))$$
$$+ v_{k-1} \cos(-\theta_{k-1} - (\pm\, 45°)) + u_{k-1} \sin(-\theta_{k-1} - (\pm 45°))]$$

$$+ 1/2\, \mathbf{n_{s\,k}}\ [z_{k-1} \sin(-\theta_{k-1} - (\pm\, 45°))$$
$$+ v_{k-1} \sin(-\theta_{k-1} - (\pm\, 45°)) + u_{k-1} \cos(-\theta_{k-1} - (\pm 45°))]$$

(15)

and

$$\sum_{L=1}^{4} \{n_L(kT)\, n'_L\, (kT-2T)\}_{\pm 45°} = [1/2\, z_k \cos(\pm\, 45° - \theta_k)$$
$$+1/2\, v_k \cos(\pm\, 45° - \theta_k) + 1/2\, u_k \sin(\pm\, 45° - \theta_k)$$
$$+ 1/2\, n_{ck} \cos(\pm\, 45°) + 1/2\, n_{sk} \sin(\pm\, 45°)] \quad \mathbf{n_{c\,k-2}}$$
$$+ [-1/2\ z_k\ \sin(\pm\, 45° - \theta_k)$$
$$- 1/2\, v_k \sin(\pm\, 45° - \theta_k) + 1/2\, u_k \cos(\pm\, 45° - \theta_k)$$
$$- 1/2\, n_{ck} \sin(\pm\, 45°) + 1/2\, n_{sk} \cos(\pm\, 45°)] \quad \mathbf{n_{s\,k-2}}$$

$$+ 1/2\, \mathbf{n_{c\,k}}\ [z_{k-2} \cos(-\theta_{k-2} - (\pm\, 45°))$$
$$+ v_{k-2} \cos(-\theta_{k-2} - (\pm\, 45°)) + u_{k-2} \sin(-\theta_{k-2} - (\pm 45°))]$$

$$+ 1/2\, \mathbf{n_{s\,k}}\ [z_{k-2} \sin(-\theta_{k-2} - (\pm\, 45°))$$
$$+ v_{k-2} \sin(-\theta_{k-2} - (\pm\, 45°)) + u_{k-2} \cos(-\theta_{k-2} - (\pm 45°))]$$

(16)

Similarly, using eq. (7) and eq. (10), we can get $\mathbf{d_{1I}(kT)}$, $\mathbf{d_{1Q}(kT)}$, **$\mathbf{d_{2I}(kT)}$ and $\mathbf{d_{2Q}(kT)}$** in **Rayleight** fading channel, or from eq.'s (14-(a,b,c,d)) by puting $\mathbf{z_k, z_{k-1} = 0}$.

Knowing the quantities $\mathbf{d_{1I}\ (kT)}$, $\mathbf{d_{1Q}\ (kT)}$, $\mathbf{d_{2I}\ (kT)}$ and $\mathbf{d_{2Q}(kT)}$, the four state **Viterbi** decoder finds the trellis path of maximum likelihood by estimating **m(k)** or **B(k)** i.e. $\Delta\theta_k$.

CONCLUSIONS

Figures (3) to (6) illustrate the average bit error probability of the 4-state **4DPSK** scheme and three different 4-state **8DPSK** schemes in **Rayleigh** fading channel and in different **shadowed Rician** fading channels respectively. The normalized fading bandwidth $\mathbf{f_D\ T}$ is chosen 0.3.

As observed, for error probabilities of 10^{-3}, or less, the 4-state **8DPSK** code with **Maximum** product of the squared branch distances and without parallel paths of Figure (2-d) i.e. 4-S **8DPSK** (2), has better performance than the other schemes.

In light shadowing the coding gain of the 4-state **8DPSK** (2) for bit error probabilities in the area of 10^{-3}, which is important in digital speech transmission, is about 0.4 and 1 dB with respect to the codes shown in Figure (2-b) and (2-c) respectively. For the lower bit error probabilities, both 4-state **8DPSK** (2) and 4-state **8DPSK** (1) codes illustrated in Figure (2-d) and (2-c) respectively, have significantly more coding gain than the 4-state -**Ungerboeck 8DPSK** code of Figure (2-b). However, the performance of the 4-state **8DPSK** (2) code is 2 dB superior to the 4-state **8DPSK** (1) at high SNR's

APPENDIX A

The normal random variate is generated from a nonlinear transformation of a uniform distribution, and is given by [12]

$$x_{G_k} = 4.91\ ((y_k)^{0.14} - (1-y_k)^{0.14}) \qquad (17)$$

where

- $\mathbf{y_k}$ is a random variate, uniformly distributed between 0 and 1.
- x_{G_k} is a Gaussian variate with zero mean and unity variance.

To convert this variate to actual mean and variance, the following transformation is required.

$$x_k = \sqrt{d}\ x_{G_k} + \mu \qquad (18)$$

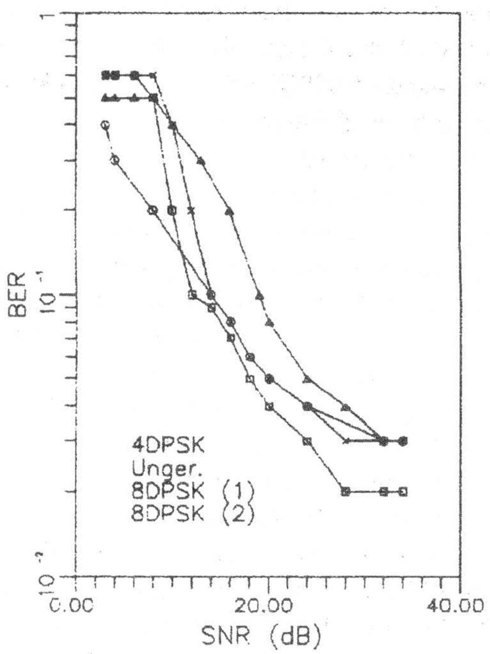

Figure 3. Comparison of the performance of 4-state **4DPSK TCM** scheme with three different 4-state **8DPSK TCM** schemes in **Rayleigh** fading channel.

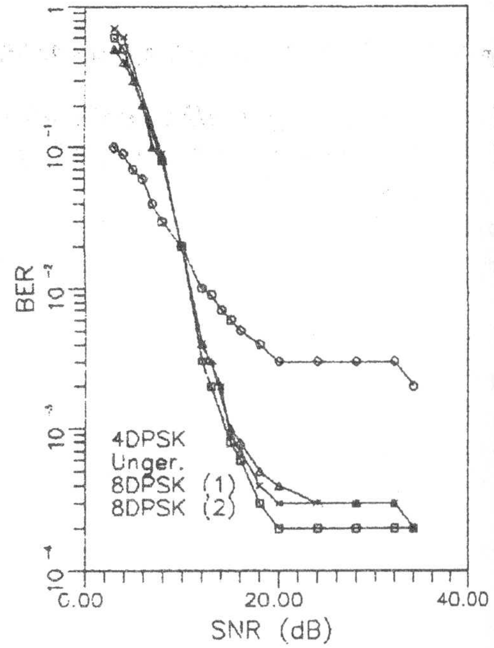

Figure 5. Comparison of the performance of 4-st **4DPSK TCM** scheme with three different 4-st **8DPSK TCM** schemes in **average** shadowing Rici fading channel.

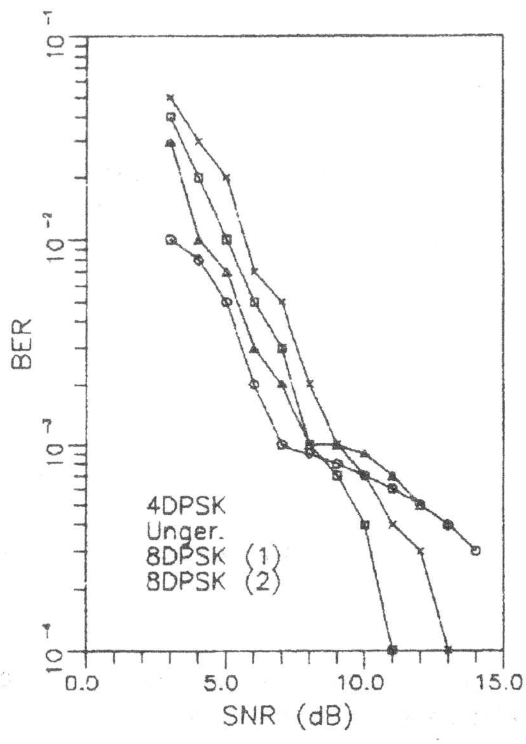

Figure 4. Comparison of the performance of 4-state **4DPSK TCM** scheme with three different 4-state **8DPSK TCM** schemes in **light** shadowing Rician fading channel.

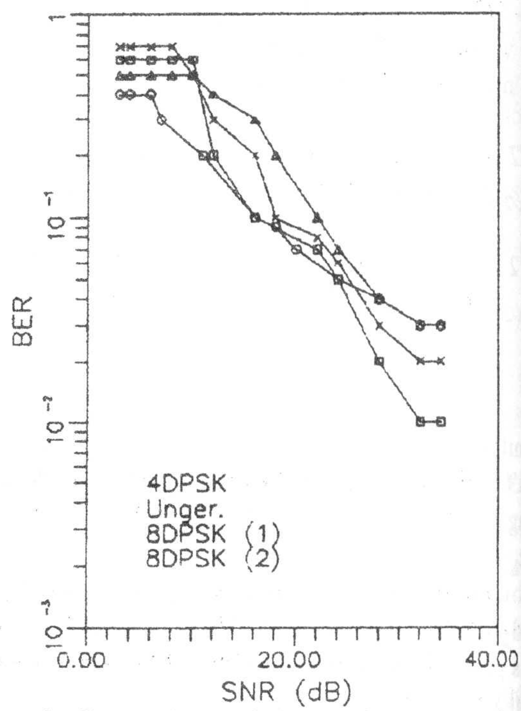

Figure 6. Comparison of the performance of 4-st **4DPSK TCM** scheme with three different 4-st **8DPSK TCM** schemes in **heavy** shadowing Ric fading channel.

where μ and $\mathbf{d}$ are the mean and variance, respectively. In the digital computer simulation program the fading model is multiplied by the generated symbols and zero mean, white Gaussian noise is then added to the **faded** signals. To simulate the channel, several sets of tones were generated: two sets of zero mean and variance $\mathbf{N_o}$ for the additive white Gaussian noise components, $\mathbf{n_{ck}}$ and $\mathbf{n_{sk}}$, two sets of zero mean and variance $\mathbf{b_o}$ for the two independent **Rayleigh** multipath components $\mathbf{v_k}$ and $\mathbf{u_k}$,

where

$$v_k = A_k \cos(2\pi (f_D + (\Delta f)_k) kT),$$

$$u_k = A_k \sin(2\pi (f_D + (\Delta f)_k) kT), \qquad (19)$$

and $\mathbf{b_0} = \sum_{k=1}^{K} \mathbf{A_k}^2 / \mathbf{K}$, **K** is the number of sinusoids.

A lognormal line-of-sight **(LOS)** component, $\mathbf{z_k}$ is added to the Rayleigh fading for **shadowed Rician** fading model, then, we generate one tone of mean μ_o and variance $\mathbf{d_0}$.

$$z_k = \exp(x_k)$$

$$= \exp\left(\sqrt{d_o}\, x_{G_k} + \mu_o\right), \qquad (20)$$

x_{G_k} is the Gaussian variate of eq. (17).

The parameters $\mathbf{b_0}$, μ_o, and $\mathbf{d_0}$ determine the degree of shadowing. Channel model parameters used in the simulation are given in Table **I**.

Table I. Channel model parameters.

	Light shadowing	Average shadowing	Heavy shadowing
d_o	0.01323	0.02592	0.64964
μ_o	0.115	-0.115	-3.91
b_o	0.158	0.126	0.0631

REFERENCES

[1] G. Ungerboeck, "channel coding With multilevel/phase signals," *IEEE Trans. On Information Theory*, p.p.55-67, Jan. 1982.

[2] H.K. Thapar, "Real-time application of trellis coding high speed voice-band data transmission," *IEEE J. Sel. Areas Commun.*, Vol. SAC-2, No. 5, p.p. 648-658, Sept. 1984.

[3] Marvin K. Simon, Dariush Divsalar, "The performance of trellis coded multilevel DPSK on a fading mobile satellite channel," *IEEE Trans. On Veh. Tech.*, Vol. 37, No. 2, p.p. 78-91, May 1988.

[4] Israel Korn, "Differential phase shift keying in two-path Rayleigh channel with adjacent channel interference," *IEEE Trans. On Veh. Tech.*, Vol. 40, No. 2, p.p. 461-471, May 1991.

[5] Yuh-Long Chen and Che-Ho Wel, " On the performance of rate 1/2 convolutional codes with QPSK on Rician fading channels," *IEEE Trans. On Veh. Tech.*, Vol. 39, No. 2, p.p. 161-170, May 1990.

[6] Chun Sum Ng, Tjeng Thiang, Fumiyuki Adachi and Kin Mun Lye, "On the error rates of differentially detected narrowband π/4-DQPSK in Rayleigh fading and Gaussian noise," *IEEE Trans. On Veh. Tech.*, Vol.42, No. 3, p.p. 259-265 August 1993.

[7] Albert C. M. Lee and Peter J. McLane, " Convolutionally interleaved PSK and DPSK trellis codes for shadowed, fast fading mobile satellite communication channels," *IEEE Trans. On Veh. Tech.*, Vol. 39, No. 1, p.p. 37-47, February 1990.

[8] W. C. Jakes, *Microwave mobile communications*, Wiley, New York 1974.

[9] E. Caples, K. Massad and T. Minor, "A UHF channel simulator for digital mobile radio," *IEEE Trans. On Vehic. Technology*, p.p. 281-289, May 1980.

[10] Chun Loo, "A statistical model for a land mobile satellite link," *IEEE Trans. On Veh. Tech.*, Vol. VT-34, No.3, p.p. 122-127, August 1985.

[11] G. Ungerboeck, "Trellis-coded modulation with redundant signal sets. Part I: Introduction," *IEEE Commun. Mag.*, Vol.25, p.p. 5-12, Feb. 1987.

[12] Rodney F. W. Coates, Gaeth J. Janacek, and Keneth V. Lever, " Monte Carlo simulation and random number generation," *IEEE Journal On Selected Areas in Commun.*, Vol. 6, No. 1, January 1988.

[13] S.O. Rice, *Mathematical analysis of random noise*, Bell Syst. Tech. J. Vol. 24, 1945.